# Electric Field and Interface Charge Extraction in Field-Plate Assisted RESURF Devices

Boni K. Boksteen, *Student Member, IEEE*, Anco Heringa, Alessandro Ferrara, *Student Member, IEEE*, Peter G. Steeneken, Jurriaan Schmitz, *Senior Member, IEEE*, and Raymond J. E. Hueting, *Senior Member, IEEE*

***Abstract*— A methodology for extracting the lateral electric field ($E_x$) in the drain extension of thin silicon-on-insulator high-voltage field-plate assisted reduced surface field (RESURF) devices is detailed including its limits and its accuracy. Analytical calculations and technology computer-aided design device modeling corresponding to experimental data are used. It is shown how to obtain trapped interface charge distributions (e.g., due to hot-carrier injection) from the extracted fields. Thus, a new method for determining the position and quantity of injected charges in the drain extension of RESURF power transistors is introduced.**

***Index Terms*— Double-diffused metal–oxide–semiconductor, electric field ($E_x$), extraction, field-plate (FP), high voltage, hot-carrier injection (HCI), interface charge, power transistor, reduced surface field (RESURF), silicon-on-insulator (SOI).**

## I. Introduction

FOR the optimization and understanding of breakdown and reliability in high-voltage (HV) MOS devices, knowledge of the lateral electric field ($E_x$) distribution in the extended drain region at reverse bias is essential. In a field-plate (FP) assisted REduced SURface Field (RESURF) device this field is determined by the doping, oxide, and field-plate construction of the extension. The field can be altered by charge trapped after Hot-Carrier Injection (HCI). To better understand the unique FP-RESURF effects, optimized field shaping typically requires the ability to analyze the field and its HCI induced changes. The noninvasive extraction of lateral field from measured $I_D - V_{DS}$ characteristics can be used, as proposed in [1] and extended in [2]. This extraction methodology is applicable to the, 1-D like, field expansion [Fig. 1(c) and (d)] found in charge gradient optimized [3] trench MOS and laterally diffused MOS devices [4]–[8]. A necessary requirement is that the drain extension is longer than five times the characteristic length $\lambda$ [Fig. 1(c)] [2], with $\lambda$ governed by the semiconductor, e.g., silicon and oxide thickness [9].

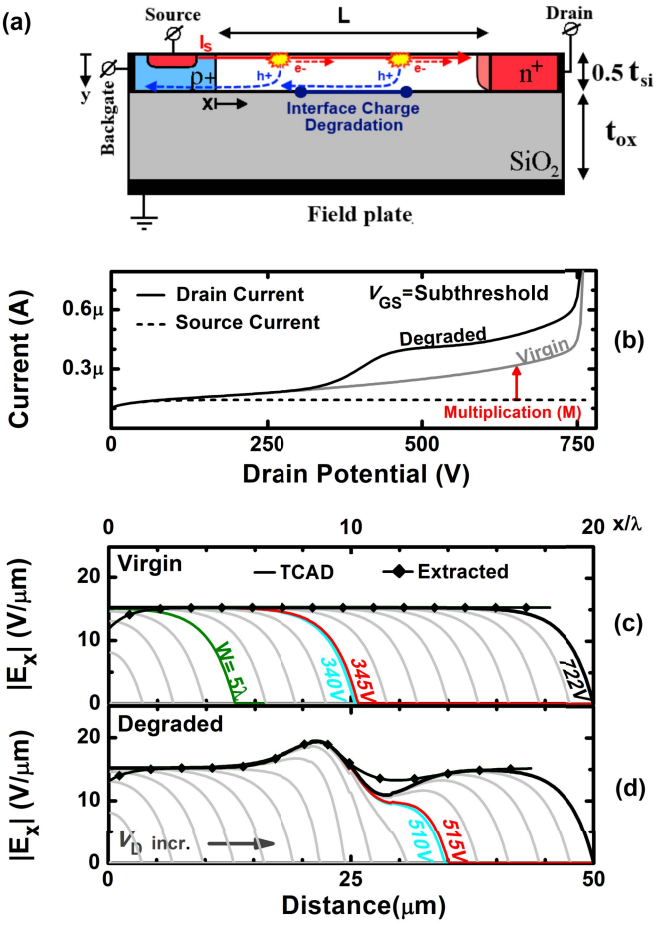


Fig. 1. (a) Half-width cross section of the studied device with interface charge, source electron current ($I_S$), electron–hole pair generation and main flow paths [1], [10] indicated in the depleted $n$-drift extension. (b) Subthreshold source and drain currents versus drain potential in an optimal (virgin) and a degraded device. The device gate width is 1000 $\mu$m. (c) and (d) TCAD modeled and extracted lateral fields for the virgin and the degraded devices. The field expansion for a (fixed $\Delta W$) $V_{DS}$ increase and the 5 $\lambda$ location [2] is also shown. The field peak and valley in the degraded device is caused by the interface charge.

Figure 1(a) shows a schematic cross section of the HV silicon-on-insulator (HV SOI) device under study. Since the oxide over the drain extension typically has approximately the same thickness as that of the buried-oxide layer, we consider

Manuscript received September 2, 2014; revised November 15, 2014; accepted December 15, 2014. Date of publication January 7, 2015; date of current version January 20, 2015. This work was supported in part by the Agentschap NL through the Dutch Point-One Program and in part by the Dutch Ministry of Economic Affairs. The review of this paper was arranged by Editor F. Udrea.

B. K. Boksteen, A. Ferrara, J. Schmitz, and R. J. E. Hueting are with the MESA+ Institute for Nanotechnology, University of Twente, Enschede 7522 NB, The Netherlands (e-mail: b.k.boksteen@utwente.nl; a.ferrara@utwente.nl; j.schmitz@utwente.nl; r.j.e.hueting@utwente.nl).

A. Heringa is with NXP Semiconductors N.V., Eindhoven 5656 AG, The Netherlands (e-mail: a.heringa@hi.nl).

P. G. Steeneken is with NXP Semiconductors N.V., Eindhoven 5656 AG, The Netherlands, and also with the Delft University of Technology, Delft 2628 CN, The Netherlands (e-mail: peter.steeneken@nxp.com).

Color versions of one or more of the figures in this paper are available online at http://ieeexplore.ieee.org.

Digital Object Identifier 10.1109/TED.2014.2383360

half a cross section in which the top surface represents the plane of symmetry. At high-drain bias, in addition to the leakage and subthreshold current, a current occurs due to impact ionization, as explained in Section II. This impact ionization current, enhanced by lateral field peaks [$E_x$, Fig. 1(c) and (d)], leads to increased drain currents ($I_D$), as shown in Fig. 1(b), which can ultimately lead to premature breakdown. The method proposed in [1] and extended in [2] was shown to provide a good way to locate these $E_x$ nonidealities.

An in-depth analysis of the details and limits of this field extraction method is still lacking. For example, how to account for the effect of $\lambda$ on the position to determine the origin of the change in impact ionization current (Section III-A), or why there are discrepancies in extracted field valleys [Fig. 1(d), Section III-B]. The objective of this paper is to provide this analysis through a combined analytical and technology computer-aided design (TCAD) [11] approach which was calibrated with experimental HCI data [1], [10]. And show how the interface charge distribution causing the changes in $E_x$ [9] can be determined.

This paper is outlined as follows. Section II presents an overview of charge-carrier multiplication and the analytical basis for field extraction. Section III discusses the extraction method and its limiting factors. Section IV presents the interface charge distribution ($N_{\rm it}(x)$) extraction. Finally, in Section V, the conclusion is drawn.

## II. Concepts of Subthreshold Multiplication and Field Extraction

In this section, we explain the core mechanisms of charge-carrier multiplication and the core concepts of the field extraction methodology. In Fig. 2(a), an ideal device with a laterally expanding block field $E_x$ is considered. It is assumed that [2]:

1) the increase in drain current is solely caused by impact ionization (II) in the depleted region;
2) an increase in depletion width $\Delta W$ caused by a change in the applied bias $\Delta V_{\rm DS}$ does not (significantly) affect the field inside the already depleted region.

This paper focuses on II currents generated in the nonreachthrough depletion range, i.e., for those drain–source voltages ($V_{\rm DS}$), where the depletion width ($W$) is less than the drain extension length ($L$). For example, Fig. 2(b) shows that $W < L = 50$ $\mu$m for $V_{\rm DS} < 730$ V. The proposed methodology is not applicable to ON-state operation (low $V_{\rm DS}$, high $V_{\rm GS}$) since then the drain extension is hardly depleted and II is not the dominant source of current.

All TCAD results shown are obtained using Silvaco Atlas [11] standard models (at 300 K). The II model used is Selberherr's model [12], with the ionization coefficients determined node by node as a function of the field in the direction of the current. These models matched multiplication changes observed through measurements in [10].

When the drain of the HV MOS device is reverse biased ($V_{\rm DS} > 0$ V) and a subthreshold gate voltage is applied, the injected source current ($I_S$) electrons [Fig. 1(a)] flow along the line of potential symmetry [3], [9]. Here, the vertical

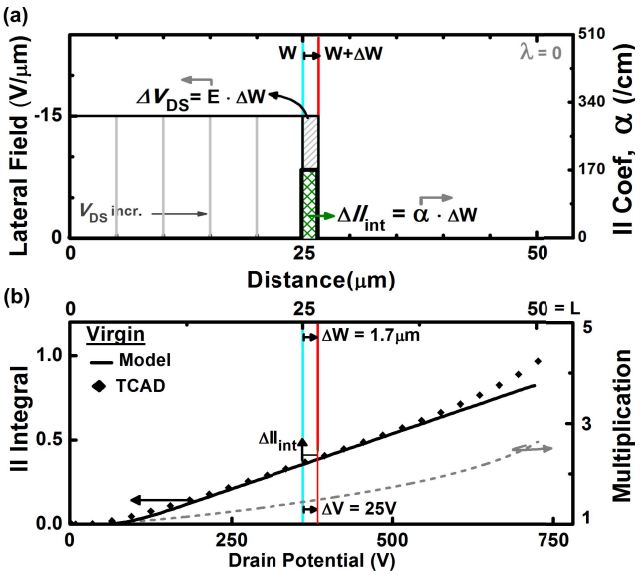


Fig. 2. (a) Left: schematic of the uniform block ($\lambda = 0$) field. Right: corresponding II coefficient expansion for a step $\Delta W$ induced by an increase in $V_{\rm DS}$. (b) Analytical [9] and TCAD obtained multiplication and II integral ($II_{\rm int}$) as a function of the drain potential (bottom axis) and depletion width (top axis) for a virgin device. Shown is the nonreachthrough condition.

field is minimal ($E_y = 0$) and $E_x$ induced generation of electron–hole pairs, by Impact Ionization (II) multiplication, is dominant [10]. The multiplication factor ($M$) is the ratio of carriers exiting the depleted drain extension (the drain current $I_D$) and those entering the depleted drain extension [at $x = 0$, Fig. 1(a), the electron source current]. With a separate back gate contact the generated holes form the back gate current ($I_{\rm Bg}$) with $I_{\rm Bg} = I_D - I_S = (M-1)\cdot I_S$. Carrier multiplication is given by

$$M(W) = M(V_{\rm DS}) = \frac{I_D(V_{\rm DS})}{I_S(V_{\rm DS})} = 1 + \frac{I_{\rm Bg}(V_{\rm DS})}{I_S(V_{\rm DS})} \tag{1}$$

where $M$ is a function of $W$, which in turn is related to the drain potential [2], [13]. For an accurate $E_x$ extraction, the subthreshold gate condition is essential as it provides a dominant supply of electrons [Fig. 1(a)]. In this case, $M$ is predominately governed by $E_x$ and the thermally generated leakage component, which induces a more complex multiplication mechanism [10], can be ignored. To study the changes in multiplication caused by HCI stress ( [10], [14], Section IV) it is best to use a fixed level carrier supply entering the device ($I_S$). This can be achieved using a fixed current criterion at a relatively low reverse bias, e.g., 0.1 nA/$\mu$m at 50 V, 100 nA [Fig. 1(b), gate width = 1000 $\mu$m], for which there is hardly any multiplication ($I_S \approx I_D$). This avoids having to perform additional $M$ normalization due to possible stress-induced threshold voltage ($V_{\rm th}$) shifts. The chosen subthreshold source current should be low to prevent Kirk-effect-like field changes.

The II-induced electron current, per unit distance $x$, used to determine $M$, is described by [15]

$$\frac{dI_n(x)}{dx} = \alpha_n(x) I_n(x) + \alpha_p(x) I_p(x) \tag{2}$$

where $I_n$ and $I_p$ are the electron and hole currents, respectively, and $\alpha_n$ and $\alpha_p$ the electron resp. hole II coefficient. The II coefficients describe the amount of electron–hole pairs generated at a certain field, per unit distance $x$ per entering carrier. For the electric field range of interest, in silicon, electron–hole pair generation is mostly caused by electrons as $\alpha_n \gg \alpha_p$. In combination with the subthreshold operation where, $I_n \gg I_p$ (at the depletion edge), the hole contribution of (2) is neglected [the Appendix, (18)].

The weighted average of coefficients $\alpha_n$ and $\alpha_p$ can be described using Fulop's approximation [16]

$$\alpha(x) = A_{\text{fit}}|E(x)|^7 \tag{3}$$

where $A_{\text{fit}}$ is a prefactor, $10^{-34}$ cm$^6 \cdot$ V$^{-7}$ [1], [2], used to fit TCAD [Fig. 2(b)] or measured results. Hence here, $\alpha \approx \alpha_n$ [1]. Fulop's power law is used as it allows for a simple analytical analysis of subthreshold field extraction. However, for more intricate dependencies, e.g., with temperature and field, the more accurate Chynoweth's-like expressions [17]–[19] can be used.

The electron–hole pair generation for a single carrier flowing across $W$ is given by the II integral ($II_{\text{int}}$) (see Appendix)

$$II_{\text{int}}(W) = \int_0^W \alpha(x)dx = \ln(M(W)) \tag{4}$$

This equation is used to relate the measured multiplication as a function of $V_{\text{DS}}$ to II caused by a single carrier [$II_{\text{int}}$, Fig. 2(b)]. This allows an overview of normalized field induced II along the full drain extension. A change $\Delta II_{\text{int}}$, as shown in Fig. 2(b), can be utilized to compare the increase in electron–hole pair generation due to a field change at any position (drain voltage) along the drain extension. Using $M$ and $I$ changes, an increasing amount of carriers flowing along $W$ is measured requiring normalization, as performed in [1] and [2], using

$$\frac{\Delta I}{I} = \frac{\Delta M}{M} = \Delta II_{\text{int}} \tag{5}$$

which can be obtained from (2) and (4). With the two assumptions at the beginning of this section, the fields responsible for the increases in $II_{\text{int}}$ caused by steps in depletion width ($\Delta W$, Fig. 2) can be extracted [1], [2]. This is achieved using

$$\Delta II_{\text{int}} \approx \alpha \cdot \Delta W = A_{\text{fit}} E_{\text{xtr}}^7 \cdot \Delta W \tag{6a}$$

giving the field extraction equation

$$E_{\text{xtr}} \approx \left(\frac{1}{A_{\text{fit}}} \cdot \frac{\Delta II_{\text{int}}}{\Delta W}\right)^{\frac{1}{7}} \tag{6b}$$

With

$$\Delta V_{\text{DS}} = E_{\text{xtr}} \cdot \Delta W \tag{7}$$

it holds that

$$\Delta I I_{\text{int}} \approx A_{\text{fit}} E_{\text{xtr}}^7 \cdot \frac{\Delta V_{\text{DS}}}{E_{\text{xtr}}} = A_{\text{fit}} {E_{\text{xtr}}}^6 \cdot \Delta V_{\text{DS}} \tag{8a}$$

giving the extracted field as a function of the applied $V_{\text{DS}}$

$$E_{\text{xtr}} = \left(\frac{1}{A_{\text{fit}}} \cdot \frac{\Delta II_{\text{int}}}{\Delta V_{\text{DS}}}\right)^{\frac{1}{6}}. \tag{8b}$$

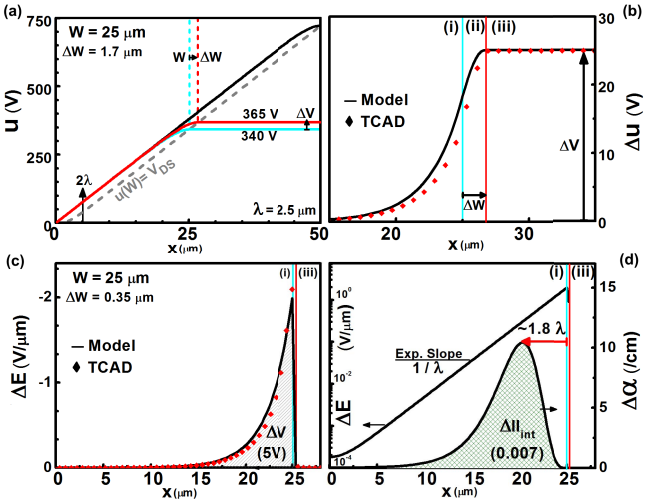


Fig. 3. (a) Lateral potential distribution ($u(x)$) for a virgin device obtained from TCAD simulations with $\lambda = 2.5$ $\mu$m for W (cyan), $W + \Delta W$ (red), and $L$ (black). Gray dashed line: modeled $W$ versus $V_{\text{DS}}$ relation. (b) Potential distribution change ($\Delta u$) for increment $\Delta W$ showing three regions of change. (c) Field distribution change ($\Delta E$) using a smaller $\Delta W$, with the change in drain potential ($\Delta V$) being the area under the curve. (d) Left axis: $\Delta E$ on log scale, showing the characteristic $e^{1/\lambda}$ falloff [9]. Right axis: II coefficient change for a $\Delta W$ showing a $1.8\,\lambda$ shifted peak, with the area under the curve the change in II integral ($\Delta II_{\text{int}}$).

The extraction location is found by

$$x_{\text{xtr}} = \frac{\Delta V_{\text{DS}}}{E_{\text{xtr}}} + W + x_{\text{cr}} \tag{9}$$

with $x_{\text{cr}}$ a correction parameter (Section III) that is zero for the ideal block field case represented in Fig. 2(a).

Applying the equations to the measured currents results in the extracted field, as shown in Fig. 1(c) and (d). The top and bottom axes of Fig. 2(b) show the link between voltage and depletion width assuming a constant field $E_x$. Since this will generally not hold, field extraction on actual measurements should be performed using (8b) and (9).

## III. Field Extraction in Reduced Surface Field (RESURF) Devices

In the depleted parts of FP assisted SOI RESURF devices, even ideal ones, a nonabrupt lateral falloff is present in the electric field [Fig. 1(c) and (d)] and potential [Fig. 3(a)], related to the so-called characteristic length $\lambda$ [9]. As a consequence, $\lambda$ determines the extent to which assumption 2) in Section II holds. With increasing $\lambda$ extraction inaccuracies appear, not present in the block field case [Fig. 2(a), $\lambda = 0$].

### A. Constant Field Case

The effect of a nonabrupt falloff ($\lambda = 2.5$ $\mu$m) will be analyzed using a constant field [virgin, Fig. 1(c)]. These fields are modeled using equations for potential distribution, as reported in [2] and [13] with TCAD extracted values of $\lambda$ [9].

From the (quasi-) 2-D Poisson equation the non-reachthrough potential distribution [Fig. 3(a)] of an ideal RESURF device along the line of potential symmetry ($y = 0$)

is given by [2], [13]

$$u_W(x) = \begin{cases} -E_{\text{sat}}\lambda\left(\dfrac{x}{\lambda} - \dfrac{\sinh\left(\dfrac{x}{\lambda}\right)}{\cosh\left(\dfrac{W}{\lambda}\right)}\right) & x < W < L \\ -E_{\text{sat}}\lambda\left(\dfrac{W}{\lambda} - \tanh\left(\dfrac{W}{\lambda}\right)\right) & W \le x < L \end{cases}$$

$$E_{\text{sat}} \approx \frac{BV_{\text{DS}}}{L} \quad \text{and} \quad u(W) = V_{\text{DS}} \tag{10}$$

with $E_{\text{sat}}$ the lateral saturation field [15 V/$\mu$m, Fig. 1(c)], $W$ the depletion edge, $\lambda$ the characteristic length [9], $BV_{\text{DS}}$ the OFF-state breakdown voltage and $L$ the drain extension length. From (10) the depletion width versus drain voltage relation $W(V_{\text{DS}})$ is obtained. This width [Fig. 3(a), dashed line] expands nearly linearly [2] for $W > 2\lambda$ as the tanh component for $u(W)$ becomes negligible. The depletion width from where the lateral field is clamped [$W \approx 5\lambda$, Fig. 1(c)] and the second extraction assumption becomes applicable, was also obtained using (10). Utilizing this $W > 5\lambda$ field clamping criterion gives insights into estimating the device breakdown voltage ranges across which the field extraction can be applied [2].

The changes $\Delta u$, $\Delta E$, and $\Delta\alpha$ for a step $\Delta W$ are shown in Fig. 3(b)–(d), respectively. These distribution changes form the core parameters necessary for field extraction (Section II). The nonabrupt lateral fall-off ($\lambda \neq 0$) results in less local $\Delta E$ and $\Delta\alpha$ changes with peak $\Delta\alpha$ changes outside the newly depleted regions [region (i), Fig. 3(c) and (d)]. To analyze the extraction errors caused by this, the potential difference distribution $\Delta u(x)$ for a change in depletion width $\Delta W$ is

$$\Delta u(x) = u_{W+\Delta W}(x) - u_W(x). \tag{11}$$

Substituting (10) in (11) results in

$$\Delta u(x) = \begin{cases} E_{\text{sat}}\lambda\sinh\left(\dfrac{x}{\lambda}\right)\left(\dfrac{1}{\cosh\left(\dfrac{W+\Delta W}{\lambda}\right)} - \dfrac{1}{\cosh\left(\dfrac{W}{\lambda}\right)}\right) & \text{(i)} \\ -E_{\text{sat}}\lambda\left(\dfrac{x-W}{\lambda} - \dfrac{\sinh\left(\dfrac{x}{\lambda}\right)}{\cosh\left(\frac{W+\Delta W}{\lambda}\right)} + \tanh\left(\dfrac{W}{\lambda}\right)\right) & \text{(ii)} \\ -E_{\text{sat}}\lambda\left(\dfrac{\Delta W}{\lambda} - \tanh\left(\dfrac{W+\Delta W}{\lambda}\right) + \tanh\left(\dfrac{W}{\lambda}\right)\right) & \text{(iii)} \end{cases} \tag{12}$$

where the drain extension is divided into three regions:

(i) the depleted region, $x < W < L$;
(ii) the region of depletion expansion, $W < x < W + \Delta W < L$;
(iii) the quasi-neutral region, $W + \Delta W \le x < L$.

Figure 3(b) shows good agreement between TCAD and analytical results for $\Delta u(x)$ across all three regions. The field change in Fig. 3(c) is the derivative ($\Delta E(x) = -(d\,\Delta u(x)/dx)$) of the potential change. The area under the curve represents the change in $V_{\text{DS}}$ while the slope, as plotted in Fig. 3(d) (left axis), shows the characteristic $e^{1/\lambda}$ falloff [9].

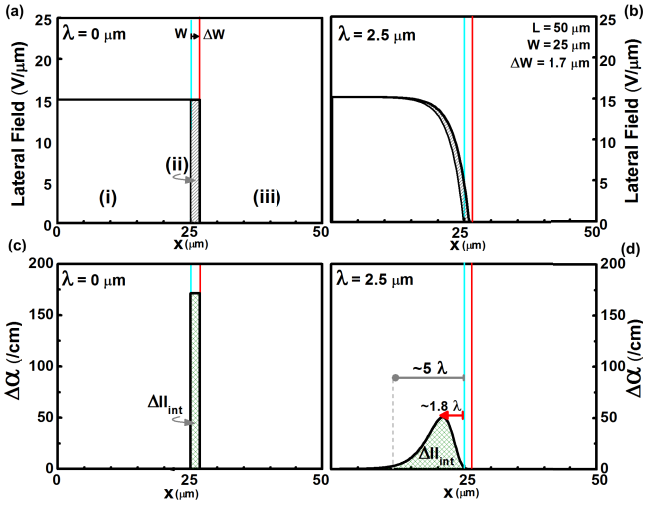


Fig. 4. Overview block field versus RESURF field. (a) and (b) Field expansion for $\Delta W = 1.7$ $\mu$m ($\approx$ 25 V). (c) and (d) Resultant $\Delta\alpha$ distributions showing $1.8\lambda$ $\Delta\alpha$ peak shift from depletion edge with effective length $\approx 5\lambda$, for $\lambda \neq 0$ case.

The lateral (field) positional resolution is the highest when the $\Delta W$ ($\Delta V$) step is infinitesimal. Keeping this in mind, changes in region (ii) can be neglected for sufficiently small steps ($\Delta W \ll \lambda$, [9]). In practice, the resolution of the measurement equipment will be the determining factor for the minimum step size $\Delta V$. If the measured current (change) is too low for the measurement equipment, a larger $\Delta I$ can be obtained for the same $\Delta V$ ($\Delta W$) by increasing the subthreshold current. However, the current should still remain low to avoid changes of $E_x$ due to high-injection effects.

The change in distribution of generated electron–hole pairs [$\Delta\alpha$, Fig. 3(d)] per carrier for a given $\Delta W$ determines the change in II integral $\Delta II_{\text{int}}$ [enclosed area, Fig. 3(d)], the key parameter for extraction (6b) and (8b). This change can be written as

$$\Delta\alpha(x) = \alpha_{W+\Delta W}(x) - \alpha_W(x) \tag{13}$$

giving

$$\Delta\alpha(x) = A_{\text{fit}}E_{\text{sat}}^7 \cdot \begin{cases} \left(\dfrac{\cosh\left(\dfrac{x}{\lambda}\right)}{\cosh\left(\dfrac{W}{\lambda}\right)} - 1\right)^7 - \left(\dfrac{\cosh\left(\dfrac{x}{\lambda}\right)}{\cosh\left(\dfrac{\Delta W+W}{\lambda}\right)} - 1\right)^7 & \text{(i)} \\ \left(1 - \dfrac{\cosh\left(\dfrac{x}{\lambda}\right)}{\cosh\left(\dfrac{\Delta W+W}{\lambda}\right)}\right)^7 & \text{(ii)} \\ 0 & \text{(iii)} \end{cases} \tag{14}$$

using Fulop's formula (3) with $E_x = -du/dx$ and ranges (i), (ii), and (iii) as mentioned previously. The modeled results are shown in Fig. 3(d), right axis. The increase in ionization integral ($\Delta II_{\text{int}}$) measured for a $\Delta W$ (or $\Delta V$) represents the area under the curve. The peak change in electron–hole pair generation does not occur at the edge of the depletion region, where the peak change in field occurs [Fig. 3(c)], but some distance before. Figure 4 shows an

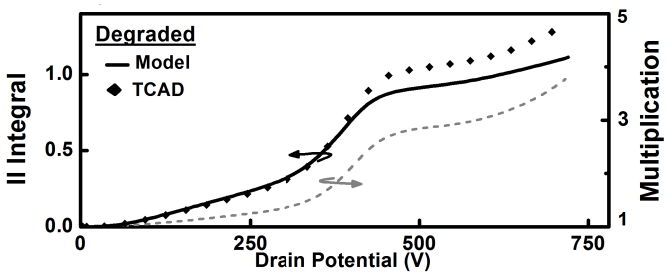


Fig. 5. Analytically [9] and TCAD obtained multiplication and II integral ($II_{\rm int}$) as a function of the drain potential for the nonconstant field (degraded) device shown in Fig. 1(b).

overview of the positional shift of the extraction location (the II current origin), between the block field and the ideal RESURF field. The peak location of change ($d\,\Delta\alpha/dx = 0$) for the latter is found to be located $1.8\,\lambda$ from the depletion edge $W$. This is because $\alpha$ is strongly dependent on the absolute field, as shown in (3). Consequently, a relatively small field change at an already high field [Fig. 4(b)] contributes more to the II process [Fig. 4(d)] than a relative large field change at a low field. This is seen in the realistic devices due to the curvature (nonzero $\lambda$) in field near the edge of the depletion region. When relating the measured II integral change ($\Delta II_{\rm int}$) to position, the shifted peak $\Delta\alpha$ contribution has to be considered to obtain the extraction location $x_{\rm xtr}$. This ($x_{\rm xtr} = W - 1.8\,\lambda$) was done for the extracted field (6b) shown in Fig. 1(c). It is of interest that the $W = 5\,\lambda$ field clamping criterion [Fig. 1(c)] [2] can also be interpreted as the (approximate) length of $\Delta\alpha$, as shown in Fig. 4(d).

### B. Nonconstant Field Case

Because a multiplication change in the nonreachthrough condition is directly related to a change in the depletion width (4), the field extraction in Section III-A, the constant field case, was performed by varying $\Delta W$ using (6b). This is only useful when the $W$ versus $V_{\rm DS}$ relation [(10), $u(W) = V_{\rm DS}$] is known. Since TCAD simulations and measurements provide the multiplication as a function of $V_{\rm DS}$ without knowing the corresponding $W$, the extraction using (8b) is more suitable.

Field extraction using the $\Delta V_{\rm DS}$ based equation (8b) is performed on the TCAD obtained $I$–$V$ characteristics of the (degraded) device [Figs. 1(b) and 5]. This results in the extracted fields shown in Fig. 6(a) with a positional shift (delay) when applying no correction (TCAD versus $x_{\rm cr} = 0$). Since the peak contribution in the measured II change, for a step $\Delta W$, was shown to have a $1.8\,\lambda$ shift [Fig. 4(d)], this correction is applied. This is insufficient as shown by the dashed line in Fig. 6(a). Due to the slower depletion expansion in the initial part of the extension, an additional $\approx 1\,\lambda$ correction is required, as shown in Fig. 6(a) (solid line). This additional shift is inherent to the $V_{\rm DS}$ method, which attributes measured multiplication changes and their corresponding extraction location (9) only to laterally expanding clamped fields. This is not the case in the initial part of the extension, i.e., prefield clamping [$W < 5\,\lambda$, Fig. 1(c)], resulting in the overestimation of extraction location requiring the additional ($\approx 1\,\lambda$) correction. A direct correction for possible extraction shifts is provided

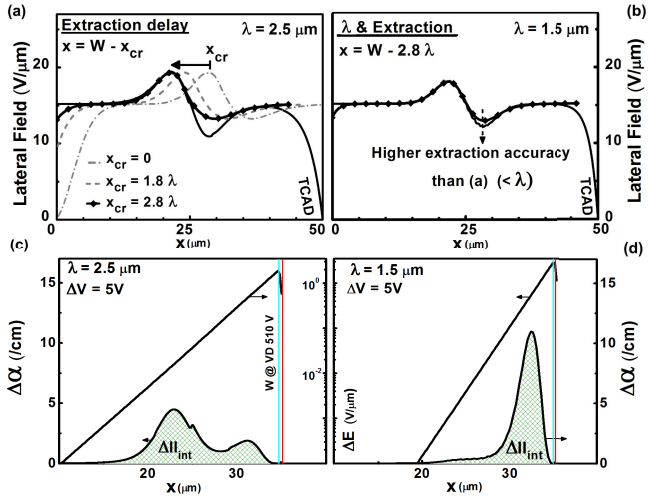


Fig. 6. (a) Extracted field of a degraded device using (8b), showing a shift in extraction position and required position correction ($x_{\rm cr}$). (b) Higher extraction accuracy for device with smaller $\lambda$. (c) and (d) Analysis of $\Delta\alpha$ at position of highest extraction discrepancy for two values of $\lambda$. A more localized $\Delta\alpha$ for smaller $\lambda$ is observed.

when the extracted field can be linked to a known physical location such as the LOCOS (local oxidation of silicon) bird's beak in the drain extension [1], [10].

In Fig. 6(a) and (b), the extracted fields of two devices with different $\lambda$'s (dielectric thicknesses) are compared. It is seen that for a lower $\lambda$ [Fig. 6(b)] the extracted field, particularly in the field valley, has better overlap. Figure 6(c) and (d) shows the corresponding $\Delta\alpha$ for a $\Delta V$ in their respective field valleys. This is caused by the nonlocal contribution, associated with the $\lambda$ related lateral falloff, of II caused by minor field changes at field peaks in the already depleted region. As shown in Fig. 6(c) versus (d), the difference in distribution of the avalanche coefficient ($\Delta\alpha$) is less influenced by these peaks and is more local for a smaller $\lambda$, and hence, a sharper field falloff ($\Delta E$). Attributing this nonlocal ($\Delta\alpha$) distribution to a single position (i.e., $\Delta II_{\rm int}$ value), as done in the extraction methodology, results in a flattening of extracted fields, which is most apparent as an extraction overestimation in field valleys [Fig. 1(d)]. For higher accuracy, an iterative method using a combination of measurement, extraction and TCAD verification is needed.

## IV. Converting Lateral Field Change to Interface Charge Profiles

Trapped charge ($Q_{\rm it} = q \cdot N_{\rm it}$) at the $Si/SiO_2$ interface caused by Hot-Carrier Injection (HCI) [10] induces field changes along the drain extension. It is therefore of interest to investigate (interface) charge induced changes using the presented field extraction methodology.

Figure 7(a) inset shows an example $II_{\rm int}$ versus $V_{\rm DS}$ evolution as obtained (4) from multiplication ($M$) increases observed [10] for subsequent (HCI) stress times [modeled by interface charge, Fig. 7(d)]: virgin case ($t = 0$), $t = t1$, and $t = t2$. Field extraction is performed to obtain the HCI induced field response [Fig. 7(a)], i.e., the field difference ($E_{\rm it}$), between the virgin field and the degraded field ($E_{\rm it} = E_{\rm t1|t2} - E_{\rm virgin}$, solid) and between the degraded

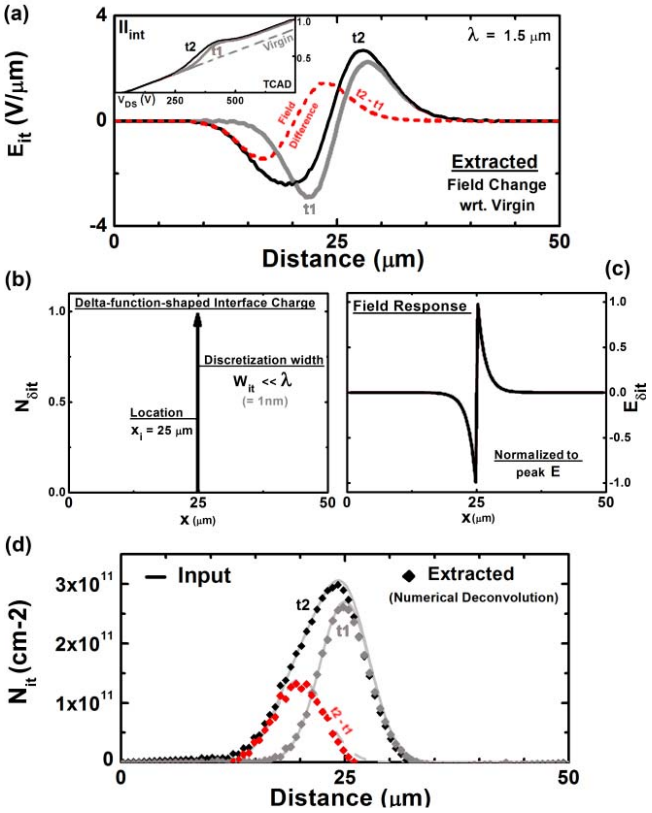


Fig. 7. (a) Extracted field change ($E_{\mathrm{it}}$) and field difference (dashed line) from $II_{\mathrm{int}}$ versus $V_{\mathrm{DS}}$ curves (inset) of devices with unknown interface charge $N_{\mathrm{it}}$. (b) Delta function shaped interface charge at position $x_i = 25\ \mu$m. (c) Corresponding field response ($E_{\delta\mathrm{it}}$). (d) Input charge distributions (lines) and extracted interface charge distributions (symbols) from the field changes of (a).

fields themselves ($E_{\mathrm{it}} = E_{\mathrm{t2}} - E_{\mathrm{t1}}$, dashed line). The response [$u_{\mathrm{it}}$ and $E_{\mathrm{it}}$, Fig. 7(a)] of an arbitrary distribution of interface charge ($N_{\mathrm{it}}$) can be approximated by the convolution (denoted as $*$) of responses ($u_{\delta\mathrm{it}}$, $E_{\delta\mathrm{it}}$) from a set of interface charges [9]. For the field response, this convolution and its corresponding (bilateral) Laplace [20] transform are [9]

$$E_{\mathrm{it}}(x) = [N_{\mathrm{it}} * E_{\delta\mathrm{it}}](x) = \mathscr{L}^{-1}\{N_{\mathrm{it}}(s) \times E_{\delta\mathrm{it}}(s)\} \quad (15)$$

where the field response to a delta-function-shaped interface charge at position $x_i$, as shown in Fig. 7(b) and (c), is

$$E_{\delta\mathrm{it,i}}(x) = \begin{cases} E_i^{\mathrm{peak}} \cdot \dfrac{\cosh\left(\dfrac{x}{\lambda}\right)}{\sinh\left(\dfrac{x_i}{\lambda}\right)} & x \le x_i \\ E_i^{\mathrm{peak}} \cdot \dfrac{\cosh\left(\dfrac{(W-x)}{\lambda}\right)}{\sinh\left(\dfrac{(W-x_i)}{\lambda}\right)} & x > x_i \\ 0 & x < 0 \vee x > W \end{cases} \quad (16)$$

with $E_i^{\mathrm{peak}}$ the peak electric field [Fig. 5(c)]

$$E_i^{\mathrm{peak}}(W_{\mathrm{it}}) = \frac{qN_{\mathrm{it}}}{C_{\mathrm{ox}}\lambda}\left(1 - e^{-\frac{W_{\mathrm{it}}}{2\lambda}}\right)$$

where $C_{\mathrm{ox}}$ is the (areal) oxide capacitance, $x_i$ the position of the delta charge, $W_{\mathrm{it}}$ the discretization width ($\ll \lambda$, [9]), and $W$ the depletion edge. The influence of HCI charges on potential is obtained by integration of the electric field [9], $u_{\mathrm{it}} = -\int E_{\mathrm{it}}\,dx$.

The analytical description of the delta response (16) combined with the extracted field responses [Fig. 7(a)] therefore allows the interface charge causing such a change to be obtained by deconvolution. A straightforward way to perform this is by deconvolution (inverse filtering) in the $s$ or $\omega$ domain and transforming the result back to the space ($x$) domain by means of the inverse (bilateral) Laplace (or Fourier) transform

$$N_{\mathrm{it}}(x) = \mathscr{L}^{-1}\left\{\frac{E_{\mathrm{it}}(s)}{E_{\delta\mathrm{it}}(s)}\right\} = \mathscr{F}^{-1}\left\{\frac{E_{\mathrm{it}}(\omega)}{E_{\delta\mathrm{it}}(\omega)}\right\} \quad (17)$$

when

$$s = j\omega.$$

Transformation to and from the $s$ or $\omega$ domain is achieved using numerical Laplace or Fourier transform packages. As such, (17) is solved by: 1) translating the analytically described $E_{\delta\mathrm{it}}(x)$ and extracted $E_{\mathrm{it}}(x)$ [(16) and Fig. 7(a)] to the $\omega$ (or $s$) domain using a Fast Fourier Transform (FFT) package; 2) performing the deconvolution (simple division) in this domain; and 3) transforming the $\omega$ domain results back to the space domain ($N_{\mathrm{it}}(\omega) \rightarrow N_{\mathrm{it}}(x)$) using an inverse FFT package [21]. The interface charge distributions causing the field changes of Fig. 7(a) as obtained using this process are shown in Fig. 7(d) and show good agreement between the TCAD (input) and extracted values.

The difference in sequentially extracted fields [Fig. 7(a), dashed line] and the corresponding extracted interface charge [Fig. 7(d)] show that for sequential subthreshold measurements the additional injected charge can be extracted. Such sequential (characterization) measurements provide valuable information for understanding and modeling how charge injection over time is related to field and position [10], under given (stress) conditions.

In this paper, a symmetric field oxide [Fig. 1(a)] structure is considered with equal top and bottom contribution of $N_{\mathrm{it}}$ to measured changes in the field. In the case of asymmetric devices [3] the difference in oxide capacitance in (16) has to be considered when attributing $N_{\mathrm{it}}$ to a particular interface.

## V. Conclusion

In this paper, a study on the extraction of the lateral electric field in the drain extension of field-plate-assisted RESURF devices is presented. By analysis of the mechanisms causing the measured ($I_D - V_{DS}$) changes, extraction inaccuracies have been discussed and methods to interpret and correct for them have been presented. A method to extract the interface charge from extracted field changes has been introduced. Together these methods provide a powerful, noninvasive way to extract and analyze hot carrier induced trapped charge from device $I_D - V_{DS}$ characteristics allowing device optimization.

## Appendix

Traditionally, the II integral is shown to be related to the multiplication factor using $II_{\mathrm{int}} = 1 - (1/M(W))$.

This is valid under the assumption that $\alpha_n = \alpha_p$ [15], [22] or when fitting breakdown values in the case of $\alpha_n \gg \alpha_p$ [23]. However, to obtain the full multiplication curves when $\alpha_n \gg \alpha_p$, a more accurate relation needs to be derived. Under this condition the right term in (2) is neglected, giving

$$\frac{dI_n}{dx} = \alpha_n \cdot I_n. \tag{18}$$

Integration gives

$$\ln(I_n) + c = \int_0^W \alpha_n dx \tag{19}$$

where $c$ is an integration constant.

Since at $x = 0$, $I_n = I_S$ (Fig. 1), $c = -\ln(I_S)$. Hence

$$I_n(x) = I_S \cdot \exp\left(\int_0^W \alpha_n dx\right) \tag{20}$$

consequently giving

$$M_n(W) = \frac{I_n(x)}{I_S} = \exp\left(\int_0^W \alpha_n dx\right) \tag{21}$$

thus resulting in

$$\ln(M(W)) = \int_0^W \alpha(x) dx = I I_{\text{int}} \tag{22}$$

as stated in (4).

## REFERENCES


[1] R. van Dalen, A. Heringa, P. W. M. Boos, A. B. van der Wal, and M. J. Swanenberg, "Using multiplication to evaluate HCI degradation in HV-SOI devices," in *Proc. 22nd ISPSD*, Jun. 2010, pp. 89–92.

[2] B. K. Boksteen, S. Dhar, A. Heringa, G. E. J. Koops, and R. J. E. Hueting, "Extraction of the electric field in field plate assisted RESURF devices," in *Proc. ISPSD*, 2012, pp. 145–148.

[3] B. K. Boksteen, A. Ferrara, A. Heringa, P. G. Steeneken, G. E. J. Koops, and R. J. E. Hueting, "Design optimization of field-plate assisted RESURF devices," in *Proc. 25th ISPSD*, May 2013, pp. 237–240.

[4] Y. C. Liang, K. P. Gan, and G. S. Samudra, "Oxide-bypassed VDMOS (OBVDMOS): An alternative to superjunction high voltage MOS power devices," *IEEE Electron Device Lett.*, vol. 22, no. 8, pp. 407–409, Aug. 2001.

[5] S. Merchant, E. Arnold, H. Baumgart, S. Mukherjee, H. Pein, and R. Pinker, "Realization of high breakdown voltage (>700 V) in thin SOI devices," in *Proc. 3rd ISPSD*, Apr. 1991, pp. 31–35.

[6] Y.-K. Leung, A. K. Paul, J. D. Plummer, and S. S. Wong, "Lateral IGBT in thin SOI for high voltage, high speed power IC," *IEEE Trans. Electron Devices*, vol. 45, no. 10, pp. 2251–2254, Oct. 1998.

[7] J. Zhu, W. Sun, Q. Qian, L. Cao, N. He, and S. Zhang, "700 V thin SOI-LIGBT with high current capability," in *Proc. ISPSD*, 2013, pp. 119–122.

[8] W. Zhang, B. Zhang, M. Qiao, L. Wu, K. Mao, and Z. Li, "A novel vertical field plate lateral device with ultralow specific on-resistance," *IEEE Trans. Electron Devices*, vol. 61, no. 2, pp. 518–524, Feb. 2014.

[9] B. K. Boksteen, A. Ferrara, A. Heringa, P. G. Steeneken, and R. J. E. Hueting, "Impact of interface charge on the electrostatics of field-plate assisted RESURF devices," *IEEE Trans. Electron Devices*, vol. 61, no. 8, pp. 2859–2866, Aug. 2014.

[10] B. K. Boksteen *et al.*, "On the degradation of field-plate assisted RESURF power devices," in *Proc. IEDM*, Dec. 2012, pp. 13.4.1–13.4.4.

[11] *ATLAS (Version: 5.18.3.R)*, Silvaco Inc., Santa Clara, CA, USA, Mar. 2012.

[12] S. Selberherr, *Analysis and Simulation of Semiconductor Devices*. New York, NY, USA: Springer-Verlag, 1984.

[13] S. Merchant, "Analytical model for the electric field distribution in SOI RESURF and TMBS structures," *IEEE Trans. Electron Devices*, vol. 46, no. 6, pp. 1264–1267, Jun. 1999.

[14] R. van Dalen *et al.*, "Hot carrier degradation of HV-SOI devices under off- and on-state current conditions," in *Proc. ISPSD*, May 2011, pp. 348–351.

[15] S. Sze and K. Ng, *Physics of Semiconductor Devices*. New York, NY, USA: Wiley, 2006.

[16] W. Fulop, "Calculation of avalanche breakdown voltages of silicon *p-n* junctions," *Solid-State Electron.*, vol. 10, no. 1, pp. 39–43, Jan. 1967.

[17] A. G. Chynoweth, "Ionization rates for electrons and holes in silicon," *Phys. Rev.*, vol. 109, no. 5, pp. 1537–1540, Mar. 1958.

[18] M. Ershov and V. Ryzhii, "Temperature dependence of the electron impact ionization coefficient in silicon," *Semicond. Sci. Technol.*, vol. 10, no. 2, p. 138, 1995.

[19] S. Reggiani *et al.*, "Measurement and modeling of the electron impact-ionization coefficient in silicon up to very high temperatures," *IEEE Trans. Electron Devices*, vol. 52, no. 10, pp. 2290–2299, Oct. 2005.

[20] A. Jeffrey and H. H. Dai, *Handbook of Mathematical Formulas and Integrals*. San Francisco, CA, USA: Academic, 2008.

[21] *Mathcad (Version: 15.0)*, Parametric Technology Corp., Needham, MA, USA, 2010.

[22] B. J. Baliga, *Fundamentals of Power Semiconductor Devices*. New York, NY, USA: Springer-Verlag, 2008.

[23] R. Van Overstraeten and H. D. Man, "Measurement of the ionization rates in diffused silicon *p-n* junctions," *Solid-State Electron.*, vol. 13, no. 5, pp. 583–608, May 1970.


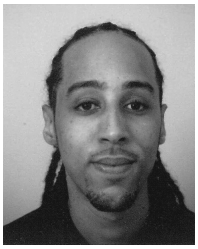

**Boni K. Boksteen** (S'10) received the M.Sc. (*cum laude*) degree in electrical engineering from the University of Twente, Enschede, The Netherlands, in 2010, where he is currently pursuing the Ph.D. degree.

He is currently involved in RESURF-based power MOS optimization and reliability with the University of Twente in collaboration with NXP Semiconductors, Eindhoven, The Netherlands.

**Anco Heringa** received the M.Sc. degree in applied physics from the University of Groningen, Groningen, The Netherlands, in 1977. He was consultant in process/device modelling with Philips until 2002. He was with NXP working on integrated high voltage devices until his retirement in 2014.

**Alessandro Ferrara** (S'12) received the master's (*cum laude*) degree in electronics engineering from the University of Naples Federico II, Naples, Italy, in 2011. He is currently pursuing the Ph.D. degree with the University of Twente, Enschede, The Netherlands.

He is currently involved in power MOS reliability with the University of Twente in collaboration with NXP Semiconductors, Eindhoven, The Netherlands.

**Peter G. Steeneken** received the M.Sc. (*cum laude*) and Ph.D. degrees in physics from the University of Groningen, Groningen, The Netherlands, in 1997 and 2002, respectively.

He has been with Philips, Eindhoven, The Netherlands, and NXP Semiconductors N.V., Eindhoven, since 2002, where he studies and develops microelectromechanical devices and power transistors. He is currently a part-time Professor of Applied Nanophysics with the Delft University of Technology, Delft, The Netherlands.

**Jurriaan Schmitz** (SM'02) received the M.Sc. degree in Physics (with honors) in 1990, and the Ph.D. degree in 1994, both from the University of Amsterdam. He worked as a Senior Scientist at Philips Research between 1994 and 2002. He is currently a Full Professor and group leader of Semiconductor Components with the University of Twente, Enschede, The Netherlands, and is Editor of Electron Device Letters.

**Raymond J. E. Hueting** (S'94–M'98–SM'06) received the M.Sc. (*cum laude*) and Ph.D. degrees in electrical engineering from the Delft University of Technology, Delft, The Netherlands.

He joined the Semiconductor Components Group, University of Twente, Enschede, The Netherlands, in 2005, where he is involved in semiconductor device physics and modeling.